

Article

Synthesis and Characterization of a New Aluminum-Doped Bismuth Subcarbonate

Loisangela Álvarez ¹, Blanca Rojas de Gascue ², Rolando J. Tremont ³, Edgar Márquez ^{4,*}  and Euclides J. Velazco ^{1,*}

¹ Laboratorio de Química Inorgánica y Catálisis, Departamento de Química, Escuela de Ciencias, Universidad de Oriente, Núcleo de Sucre, Cumaná 6101, Venezuela

² Laboratorio de Polímeros, Departamento de Materiales, Instituto de Investigaciones en Biomedicina y Ciencias Aplicadas “Dra. Susan Tai”, Universidad de Oriente, Cumaná 6101, Venezuela

³ Department of Chemistry, University of Puerto Rico at Humacao, Call Box 860, 00792 Humacao, Puerto Rico

⁴ Grupo de Investigaciones en Química y Biología, Departamento de Química y Biología, Facultad de Ciencias Básicas, Universidad del Norte, Carrera 51B, Km 5, vía Puerto Colombia, Barranquilla 081007, Colombia

* Correspondence: ebrazon@uninorte.edu.co (E.M.); evelazco@udo.edu.ve (E.J.V.)

Received: 17 July 2019; Accepted: 23 August 2019; Published: 6 September 2019



Abstract: A new compound, $\text{Bi}_2\text{O}_2\text{CO}_3:\text{Al}$, was synthesized by the coprecipitation method. The characterization was done by X-ray diffraction (XRD), Fourier transformed infrared spectroscopy (FTIR), X-ray photoelectron spectroscopy (XPS), electronic scanning microscopy (SEM), and energy dispersive X-ray spectroscopy (EDX). The characterization methods allowed to identify the $\text{Bi}_2\text{O}_2\text{CO}_3:\text{Al}$ compound, such as the Al-doped $\text{Bi}_2\text{O}_2\text{CO}_3$ by XRD, the anionic part (CO_3^{2-}) by FTIR, and the presence of aluminum in the compound by XPS and EDX. It was confirmed to have a nanostructure like a nanosheet and a microstructure that resembles a type sponge by SEM.

Keywords: $\text{Bi}_2\text{O}_2\text{CO}_3:\text{Al}$; doped; aluminum; photocatalysis

1. Introduction

Bismuth-containing compounds and presenting layered structure have attracted attention for their excellent photocatalytic properties under solar light. From this type of compounds, $\text{Bi}_2\text{O}_2\text{CO}_3$ has a layered structure similar to laminar double hydroxides, which is presented as an arrangement of units $(\text{Bi}_2\text{O}_2)^{2+}$ with the CO_3^{2-} ions located in the interlaminal zone [1]. This kind of compounds is known as a “sillén” phase, with the general formula $[\text{Bi}_2\text{O}_2] [\text{X}_m]$ (X = halogen or other ion group), alternating $[\text{Bi}_2\text{O}_2]^{2+}$ and X^n- sheets, which show very high stability at oxidizing environment [2]. $\text{Bi}_2\text{O}_2\text{CO}_3$ has been an excellent material with varied applications, especially for its remarkable optical and photocatalytic properties in reactions performed under UV and visible light [3–8].

Four essential nanostructures have been reported for the compound $\text{Bi}_2\text{O}_2\text{CO}_3$: nanoparticles [9], nanotubes [10], nanoplates [11], and nanosheets [3]. On the other hand, microstructures have been reported with four basic types of morphologies [12]: sponge [5], rose [13], flower [14], and persimmon [15]. These variations in the basic nano and microstructures of $\text{Bi}_2\text{O}_2\text{CO}_3$ can be achieved according to the type of synthetic method used (solvothermal, hydrothermal, reflux, etc.), the type of solvent (water, glycerol, ethylene glycol, etc.), the nature of the precursor of Bi^{3+} (bismuth citrate, bismuth nitrate, etc.), or the reagents used (urea, ammonium carbonate, cetyltrimethylammonium bromide, sodium citrate, etc.) [4,9–11,15,16].

The typical synthesis of $\text{Bi}_2\text{O}_2\text{CO}_3$ has been, mainly, reported under hydrothermal conditions [3,17]. Since $\text{Bi}_2\text{O}_2\text{CO}_3$ has a wide gap (3.1 to 3.5 eV), it can be easily activated with UV light, so that doping improves its photocatalytic activity towards the visible range [18]. Previous studies have reported

the synthesis of $\text{Bi}_2\text{O}_2\text{CO}_3$ doped with nitrogen [19–21], europium [8], carbon [22], lanthanum [23], iron [24], bromine [25], palladium [26], iodine [27,28], sulfur and antimony [6], that have enhanced the photocatalytic properties of $\text{Bi}_2\text{O}_2\text{CO}_3$ under visible light. However, it is also expected $\text{Bi}_2\text{O}_2\text{CO}_3$ that own hierarchical structure assembled by nanosheets or nanoplates show more active photocatalysis [2]. Velazco et al. [29] reported the synthesis of $\text{Bi}_2\text{O}_2\text{CO}_3$ doped with Al for its use as an additive for the crystallization of the CaCO_3 polymorphs, without further characterization details than X-ray diffraction and scanning electron microscopy. In the present work, the preliminary results of the characterization of aluminum-doped bismuth subcarbonate ($\text{Bi}_2\text{O}_2\text{CO}_3:\text{Al}$) are reported, which is expected to obtain a compound with an improvement photocatalytic activity; for example, in potential applications in environmental remediation process.

2. Materials and Methods

2.1. Synthesis of Al-Doped $\text{Bi}_2\text{O}_2\text{CO}_3$

All the reagents were of analytical grade and used without further purification. The Al-doped $\text{Bi}_2\text{O}_2\text{CO}_3$ was synthesized by a coprecipitation method, according to the procedure followed in the literature [29]. An aqueous solution containing 0.12 mol of bismuth nitrate pentahydrate ($\text{Bi}(\text{NO}_3)_3 \cdot 5\text{H}_2\text{O}$) and 0.04 mol of aluminum nitrate nonahydrate ($\text{Al}(\text{NO}_3)_3 \cdot 9\text{H}_2\text{O}$) was prepared in a volumetric flask lined with deionized water, in such a way to have a 3:1 ratio of Bi:Al. This solution was added to a beaker and 20 mL of deionized water were added. The pH was adjusted to 10 with a 0.80 mol/L Na_2CO_3 solution added and the reaction mixture was placed under constant stirring for 4 hours at 60 °C. The white precipitate formed was washed several times with deionized water and dried in an oven for 12 h at 80 °C.

2.2. Characterization of $\text{Bi}_2\text{O}_2\text{CO}_3:\text{Al}$

The crystal structure of $\text{Bi}_2\text{O}_2\text{CO}_3:\text{Al}$ was identified by powder X-ray diffraction, through a PANalytical diffractometer model X'Pert Pro, with a radiation $K\alpha\text{Cu} = 1.5418 \text{ \AA}$, operated at 45 kV and 40 mA, in a range $2\theta^\circ$ between 5° and 100° , with a step size of 0.02° every 20 s.

The $\text{Bi}_2\text{O}_2\text{CO}_3:\text{Al}$ was characterized by Fourier Transform Infrared spectroscopy in order to identify the bands of the anionic component. This analysis performed on a spectrophotometer Perkin-Elmer, Frontier model in KBr pellet. Surface analysis was carried out by X-ray Photoelectron Spectroscopy (XPS). The XPS spectra obtained with a multi-technique surface analysis system of Physical Electronics (Model 5600 ci) equipped with a hemispheric analyzer, a toroidal monochromator, and a multichannel detector. The pressure in the chamber during analyzes was less than 1×10^{-9} Torr.

Monochromatic Al $K\alpha$ radiation (at 350 W and 15 kV) was used for high-resolution excitation and in the survey analyzes. The binding energy values (B.E.) were corrected using the C1s signal of atmospheric pollution (285.0 eV). However, the survey and high-resolution spectra are presented as they obtained. The high-resolution spectra were recorded at a take-off angle of 45° and an energy step of 11.75 eV. The low-resolution spectra used an energy step of 93.0 eV.

The relationship of constituent elements and the morphological study achieved in an Oxford energy dispersive X-ray spectrometer (EDX), INCA X-sight coupled to a JEOL scanning electron microscope (SEM), JSM-6390, with a detection time of 1 min and an acceleration voltage of 25 kV.

3. Results

3.1. X-rays Diffraction

Figure 1 shows the X-rays diffraction pattern obtained for the compound $\text{Bi}_2\text{O}_2\text{CO}_3:\text{Al}$. The identification made by X-ray diffraction corresponds to a distinct phase of $\text{Bi}_2\text{O}_2\text{CO}_3$, this when compared with the standard of the ICDD PDF card No. 00-025-1464, which suggests that Al ions has replaced Bi's atomic positions and uniformly dispersed within the crystalline structure of $\text{Bi}_2\text{O}_2\text{CO}_3$

without altering the structure of this subcarbonate, demonstrating that the addition of Al did not influence the crystalline phase. The analysis of the (004) and (110) diffraction peaks (see Figure 1) showed the calculated lattice spacing of 3.423 Å and 2.752 Å, respectively, and they are in agreement with the spacing of $d_{004} = 3.42$ Å and $d_{110} = 2.73$ Å of $\text{Bi}_2\text{O}_2\text{CO}_3$ reported [1]. It is apparent that good crystals of $\text{Bi}_2\text{O}_2\text{CO}_3:\text{Al}$ were successfully synthesized. Also, the X-rays diffraction pattern showed NaNO_3 as impurity that could not be removed from the compound and which was obtained as sub-product during the synthesis.

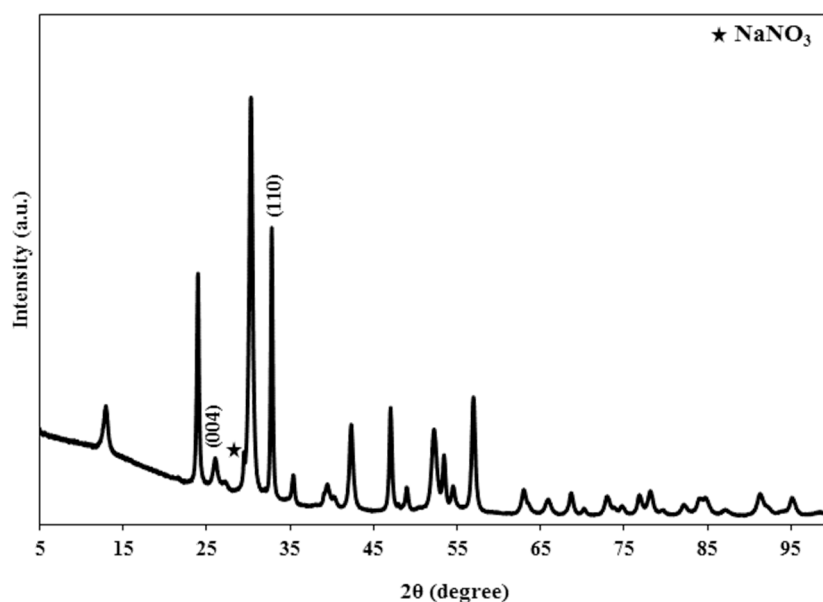


Figure 1. X-ray diffraction pattern of $\text{Bi}_2\text{O}_2\text{CO}_3:\text{Al}$.

3.2. Fourier Transform Infrared Spectroscopy

Figure 2 shows the FTIR spectrum of the compound $\text{Bi}_2\text{O}_2\text{CO}_3:\text{Al}$, with the corresponding absorption bands tabulated in Table 1. The measurement of the FTIR spectrum was performed to confirm the anionic part (CO_3^{2-}) of the compound $\text{Bi}_2\text{O}_2\text{CO}_3:\text{Al}$.

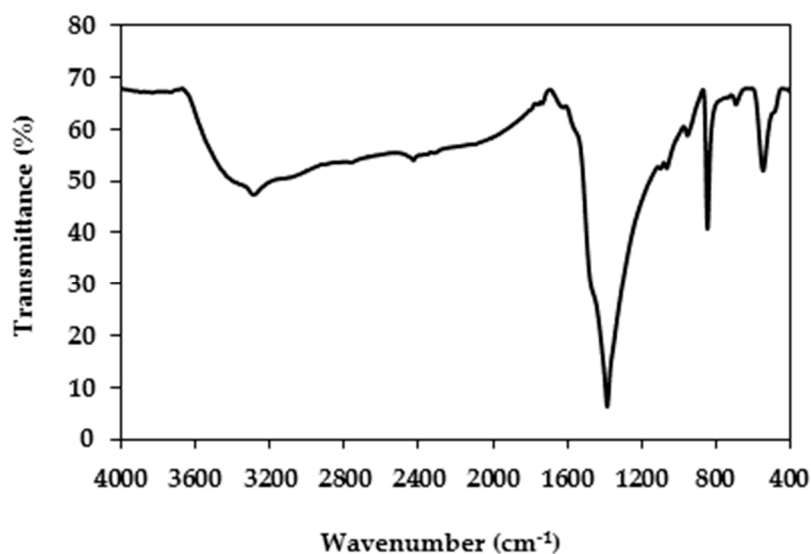


Figure 2. FTIR spectrum of the compound $\text{Bi}_2\text{O}_2\text{CO}_3:\text{Al}$.

Table 1. Main absorption bands in the IR of the compound $\text{Bi}_2\text{O}_2\text{CO}_3:\text{Al}$.

Frequency (cm^{-1})	Assignment
3292	Stretching vibration of H_2O
1477, 1385	Anti-symmetric vibration ν_3 of CO_3^{2-}
1066	Symmetric stretching vibration ν_1 of CO_3^{2-}
846	Out-of-plane bending ν_2 of CO_3^{2-}
690	In-plane deformation ν_4 of CO_3^{2-}
546	Stretching vibration of $\text{Bi}=\text{O}$

The free carbonate ion, with a point group symmetry D_{3h} , has four modes of internal vibrations [30], which were detected by IR: symmetric stretching mode ν_1 , which appeared at 1066 cm^{-1} ; the corresponding antisymmetric vibration ν_3 , observing bands at 1477 and 1385 cm^{-1} ; the out-of-plane bending ν_2 , which notes at 846 cm^{-1} ; and the in-plane deformation ν_4 , observed at 690 cm^{-1} . Even these results are in agreement with those found for the compound $\text{Bi}_2\text{O}_2\text{CO}_3$, which confirms the presence of the CO_3^{2-} ion, only the antisymmetric vibrations ν_3 showed a slight shift in the frequencies according to literature data (1468 and 1391 cm^{-1}) [13,31]. This can be attributed by change of the Bi-O-Bi-O-Bi to Bi-O-Al-O-Bi arrangement in $\text{Bi}_2\text{O}_2\text{CO}_3$, which changed the effect of interaction with CO_3^{2-} ions. On the other hand, the band at 546 cm^{-1} is attributed to the $\text{Bi}=\text{O}$ stretching, while the band between 3000 and 3700 cm^{-1} must correspond to the H-O stretching vibration of chemisorbed or physisorbed water molecules. AL-Majthoub and Refat [32] reported some bismuth subcarbonates with the formula $\text{Bi}_2\text{O}_2\text{CO}_3 \cdot 3\text{H}_2\text{O}$, which were synthesized by the reaction of aqueous solutions of urea with various bismuth(III) salts at high temperature. They found that the compounds were hydroscopic and the H_2O molecules came from moisture water.

3.3. X-ray Photoelectron Spectroscopy, XPS

The analysis by XPS of all the elements present in the sample was performed, except for H, since this did not observe in this technique. Figure 3 shows the spectrum obtained for the compound $\text{Bi}_2\text{O}_2\text{CO}_3:\text{Al}$. In addition to the XPS signals, the Auger transitions are also observed (for C KLL and O KLL). Table 2 shows the four regions detected by XPS per element. It can observe in the atomic percentages that the Bi and the Al are in a proportion of approximately 2:1, in terms of the total concentration detected of each one. However, it must remember that the XPS measures correspond to surface analysis and do not necessarily express the total content of the sample. Next, the high-resolution analysis performed per detected element.

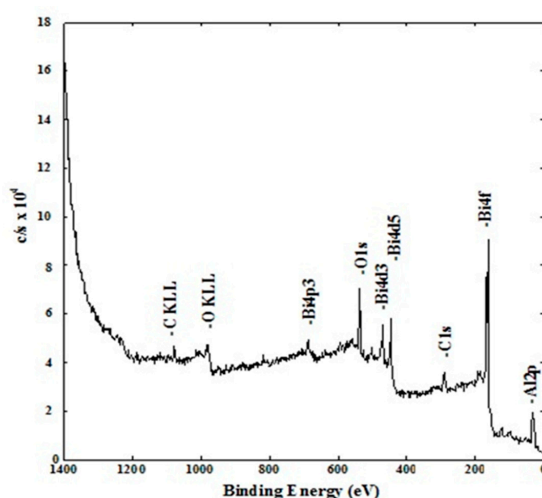
**Figure 3.** XPS spectrum for the compound $\text{Bi}_2\text{O}_2\text{CO}_3:\text{Al}$.

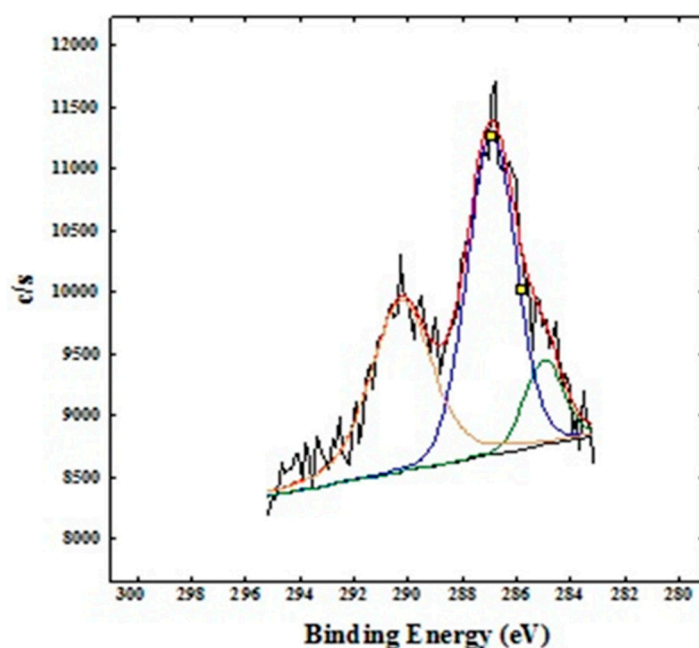
Table 2. Atomic concentration of the regions detected by XPS.

Element	% Atomic
C1s	30.44
O1s	50.21
Al2p	6.49
Bi4f	12.85

3.4. High Resolution XPS Analysis Per Element

3.4.1. C1s Region

Figure 4 shows the high-resolution XPS spectrum for the C1s region, where the presence of three peaks is observed at 285.0, 287.0, and 290.2 eV. The total concentration for C1s is 30.44%. From this total amount, the concentrations of the three signals are shown in Table 3. Of the three signals of C1s detected, those centered at 285.0 and 287.0 eV could attribute to carbon species acquired from environmental contamination during the measurements of XPS [14,19,22,33]. On the other hand, the signal at 290.2 eV is attributable to the ion CO_3^{2-} present in the sample [22,33]. This result confirms what is obtained by FTIR, where the anion present in the compound $\text{Bi}_2\text{O}_2\text{CO}_3:\text{Al}$ is the carbonate ion.

**Figure 4.** XPS spectrum for the C1s region for the compound $\text{Bi}_2\text{O}_2\text{CO}_3:\text{Al}$.**Table 3.** Atomic concentrations and assignments for the C1s region for the compound $\text{Bi}_2\text{O}_2\text{CO}_3:\text{Al}$.

Bond Energy for C1s (eV)	% by Type of C1s	Assignment
285.0	10.72	C-C, C-H Carbon from environmental contamination.
287.0	50.52	Some kind of C different to C-C, C-H
290.2	38.76	CO_3^{2-}

3.4.2. O1s Region

Figure 5 shows the high-resolution XPS spectrum for the O1s region, observing the presence of three peaks at 531.8, 533.2, and 534.8 eV. The total concentration for O1s is 50.21%. From this total amount, the atomic concentrations of the three signals are presented in Table 4. The signal at 531.8 eV

initially attributes to the species AlO(OH); however, this did not detect by x-ray diffraction. Then, it assumed that this signal must attribute to the chemical environment of Al in the laminar structure of the compound $\text{Bi}_2\text{O}_2\text{CO}_3:\text{Al}$, in the arrangement Bi-O-Al-O-Bi. The presence of H_2O corresponds to that chemisorbed or physisorbed on the surface of the compound $\text{Bi}_2\text{O}_2\text{CO}_3:\text{Al}$, whose signal is detected at 534.8 eV and which was also detected by FTIR. The signal at 533.2 eV corroborates what has been observed in the C1s signal, the presence of CO_3^{2-} in the sample [22,33].

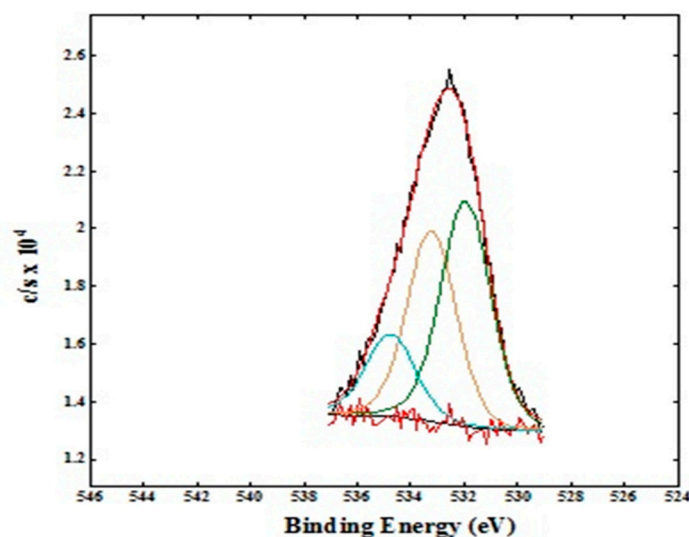


Figure 5. XPS spectrum for the O1s region for the compound $\text{Bi}_2\text{O}_2\text{CO}_3:\text{Al}$.

Table 4. Atomic concentrations and assignments for the O1s region for the compound $\text{Bi}_2\text{O}_2\text{CO}_3:\text{Al}$.

Bond Energy for O1s (eV)	% by Type of O1s	Assignment
531.8	38.66	AlO(OH)
533.2	41.22	CO_3^{2-}
534.8	20.12	H_2O

3.4.3. Al2p Region

High-resolution XPS spectrum for the Al2p region exhibits in Figure 6. In this spectrum, two signals can observe at 75.8 and 77.3 eV. The total concentration for Al2p is 6.49%. The atomic concentrations of the different signals are shown in Table 5. The more prominent presence of Al is as the species AlO(OH), with 92.11%, detected at 75.8 eV, which is originated by Al^{3+} . However, as argued for the O1s region, this species was not detected by XRD, which must correspond to the chemical environment of Al^{3+} in the compound $\text{Bi}_2\text{O}_2\text{CO}_3:\text{Al}$, in the Bi-O-Al-O-Bi arrangement. This result suggests the presence of Al-O bond in the compound $\text{Bi}_2\text{O}_2\text{CO}_3:\text{Al}$. The compound Al_2O_3 was also observed, which could be due to oxidation of residual Al present in the compound.

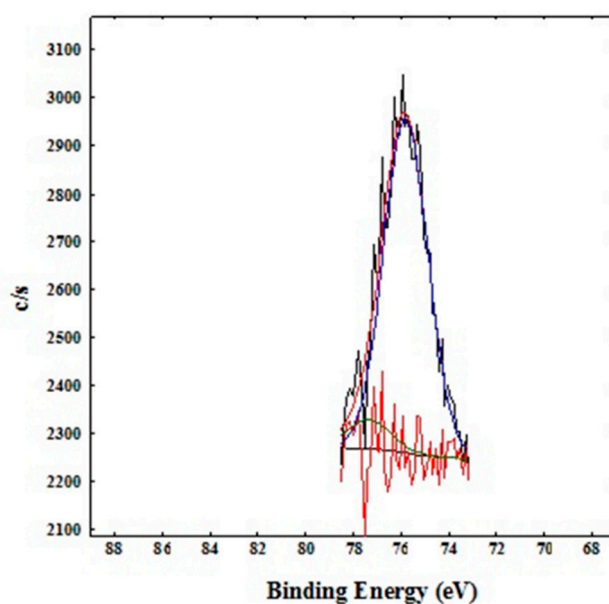


Figure 6. XPS spectrum for the Al2p region for the compound $\text{Bi}_2\text{O}_2\text{CO}_3:\text{Al}$.

Table 5. Atomic concentrations and allocations for the Al2p region for the compound $\text{Bi}_2\text{O}_2\text{CO}_3:\text{Al}$.

Bond Energy for Al2p (eV)	% by Type of Al2p	Assignment
75.8	92.11	AlO(OH)
77.3	07.89	Al ₂ O ₃

3.4.4. Bi4f Region

Figure 7 shows the high-resolution XPS spectrum for the Bi4f region for the compound $\text{Bi}_2\text{O}_2\text{CO}_3:\text{Al}$. There are two sharp characteristic symmetric peaks for the spin-orbital splitting of Bi4f peaks. The total concentration for Bi4f is 12.85% (Table 6). In this case, a binary signal obtained for a single type of chemical environment for the bismuth. These signals correspond to the states $\text{Bi}4f_{7/2}$ and $\text{Bi}4f_{5/2}$, which are originated by Bi^{3+} . As this bond energy is greater than the energy for Bi_2O_3 (159.3 eV), it can assign to a chemical environment with oxygen and aluminum, which means that this chemical environment for bismuth is of higher ionic character [22,31,33].

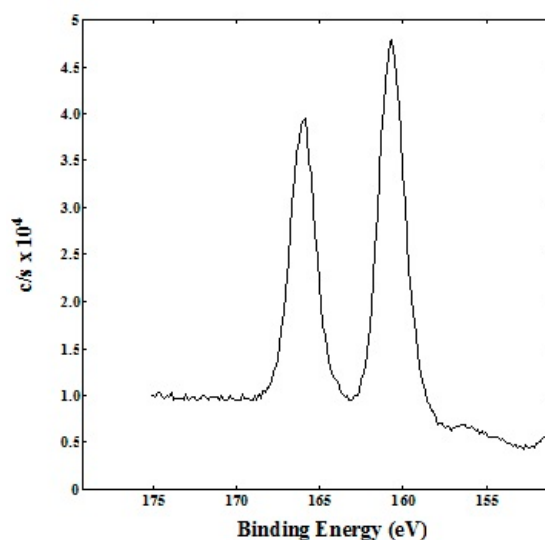


Figure 7. XPS spectrum for the Bi4f region for the compound $\text{Bi}_2\text{O}_2\text{CO}_3:\text{Al}$.

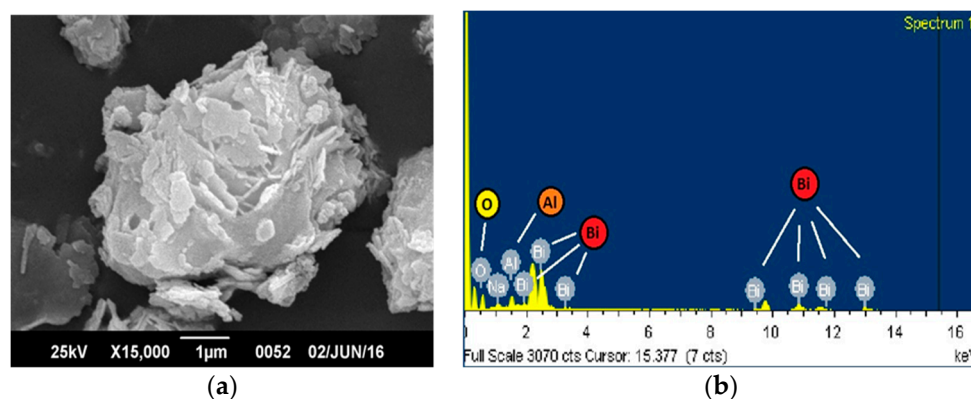
Table 6. Atomic concentrations and assignments for the Bi4f region for the compound Bi₂O₂CO₃:Al.

Bond Energy for Bi4f (eV)	%Bi4f	Assignment
160.2	12.85	Bond energy greater than that of Bi ₂ O ₃ (159.3 eV). It can be assigned to a chemical environment with oxygen and aluminum. This means that this chemical environment for bismuth is of greater ionic character.

3.5. Scanning Electron Microscopy (SEM) and Energy Dispersive X-ray Spectroscopy (EDX)

The morphological characterization of Bi₂O₂CO₃:Al compounds was carried out by scanning electron microscopy. As mentioned, four essential nanostructures have been reported for the compound Bi₂O₂CO₃ [3,9,11], while microstructures with four primary morphologies have been reported [11]. The incidence of these morphologies is intimately related to the synthesis conditions of Bi₂O₂CO₃, where most of them are subject to hydrothermal or solvothermal conditions. In addition to the reaction conditions, other factors such as solvent (water, ethanol, ethylene glycol, and others), type of reactants (nitrates, chlorides, and acetates) or base (NaOH, NH₄OH, and urea) can be decisive in the control of the morphology of Bi₂O₂CO₃. The synthesis conditions in this work were based on the controlled precipitation of bismuth nitrate and aluminum nitrate in the aqueous medium.

According to Figure 8a, the SEM image shows a characteristic laminar aggregation or stacking of Bi₂O₂CO₃, with an aggregate size between 5 and 10 μm and irregular shape. Based on the micrograph, it could suggest that the compound Bi₂O₂CO₃:Al crystallized with a nanostructure of the nanosheet type. On the other hand, the microstructure is not entirely defined with the typical ones obtained for Bi₂O₂CO₃; however, its morphology tends to resemble a sponge-type. The qualitative analysis performed by EDX (Figure 8b) confirms the presence of Al in the compound Bi₂O₂CO₃, which certifies the formation of the doped compound.

**Figure 8.** (a) SEM image, (b) EDX spectrum obtained for Bi₂O₂CO₃:Al.

4. Conclusions

In summary, Bi₂O₂CO₃ doped with Al was synthesized by a simple method of controlled precipitation in aqueous solution, allowing a compound presenting a nanostructure of nanosheets and a microstructure with a morphology resembling a sponge-type, which was revealed by SEM analysis. The formation of this microstructure can be ascribed to the aggregation of numerous nanosheets. The presence of aluminum in the lattice of Bi₂O₂CO₃ was confirmed by XPS, suggesting the presence of the Al-O bond substituting for bismuth atoms in the Bi-O-Al-O-Bi arrangement. Studies are still currently being carried out to evaluate the effect of aluminum over the optical and photocatalytic properties of Bi₂O₂CO₃.

Author Contributions: Conceptualization, E.M. and E.J.V.; methodology, L.Á., B.R.d.G., R.J.T., E.M. and E.J.V.; validation, B.R.d.G., R.J.T., E.M. and E.J.V.; formal analysis, L.Á., E.M. and E.J.V.; investigation, L.Á., B.R.d.G., R.J.T., E.M. and E.J.V.; resources, E.M. and E.J.V.; data curation, B.R.d.G., R.J.T., E.M. and E.J.V.; writing—original draft preparation, E.M. and E.J.V.; writing—review and editing, E.M. and E.J.V.; visualization, E.M. and E.J.V.; supervision, E.M. and E.J.V.; project administration, E.M. and E.J.V.

Funding: This research received no external funding.

Acknowledgments: The authors would like to acknowledge the Microscopy Center of the Universidad Simón Bolívar, Caracas, Venezuela, for the Scanning Electronic Microscopy and X-rays Dispersive Energy Spectroscopy, and the use of facilities of the Materials Characterization Center of the University of Puerto Rico, as well as the collaboration of Ramonita Diaz-Ayala with the XPS and XRD analyses. The authors also acknowledge the Department of Chemistry, University of Puerto Rico, Humacao Campus, Puerto Rico for the use of their equipment.

Conflicts of Interest: The authors declare no conflict of interest.

References

1. Huang, H.; Tian, N.; Jin, S.; Zhang, Y.; Wang, S. Syntheses, characterization and nonlinear optical properties of a bismuth subcarbonate $\text{Bi}_2\text{O}_2\text{CO}_3$. *Solid State Sci.* **2014**, *30*, 1–5. [[CrossRef](#)]
2. Liu, Y.; Wang, Z.; Huang, B.; Yang, K.; Zhang, X.; Qin, X.; Dai, Y. Preparation, electronic structure, and photocatalytic properties of $\text{Bi}_2\text{O}_2\text{CO}_3$ nanosheet. *Appl. Surf. Sci.* **2010**, *257*, 172–175. [[CrossRef](#)]
3. Zhao, T.; Zai, J.; Xu, M.; Zou, Q.; Su, Y.; Wang, K.; Qian, X. Hierarchical $\text{Bi}_2\text{O}_2\text{CO}_3$ microspheres with improved visible-light-driven photocatalytic activity. *CrystEngComm* **2011**, *13*, 4010–4017. [[CrossRef](#)]
4. Chen, R.; Cheng, G.; So, M.H.; Wu, J.; Lu, Z.; Che, C.M.; Sun, H.; Wang, C.; Zhao, Z.; Luo, B.; et al. Hierarchical $\text{Bi}_2\text{O}_2\text{CO}_3$ microspheres with improved visible-light-driven photocatalytic activity. *CrystEngComm* **2010**, *13*, 1–10.
5. Zhao, H.; Tang, J.; Lai, Q.; Cheng, G.; Liu, Y.; Chen, R. Enhanced visible light photocatalytic performance of Sb-doped $(\text{BiO})_2\text{CO}_3$ nanoplates. *Catal. Commun.* **2015**, *58*, 190–194. [[CrossRef](#)]
6. Wang, C.; Zhao, Z.; Luo, B.; Fu, M.; Dong, F. Tuning the Morphological Structure and Photocatalytic Activity of Nitrogen-Doped $(\text{BiO})_2\text{CO}_3$ by the Hydrothermal Temperature. *J. Nanomater.* **2014**, *2014*, 1–10.
7. Tang, J.; Cheng, G.; Zhou, H.; Yang, H.; Lu, Z.; Chen, R. Shape-Dependent Photocatalytic Activities of Bismuth Subcarbonate Nanostructures. *J. Nanosci. Nanotechnol.* **2012**, *12*, 4028–4034. [[CrossRef](#)]
8. Chen, R.; Cheng, G.; So, M.H.; Wu, J.; Lu, Z.; Che, C.M.; Sun, H. Bismuth subcarbonate nanoparticles fabricated by water-in-oil microemulsion-assisted hydrothermal process exhibit anti-Helicobacter pylori properties. *Mater. Res. Bull.* **2010**, *45*, 654–658. [[CrossRef](#)]
9. Chen, R.; So, M.H.; Yang, J.; Deng, F.; Che, C.M.; Sun, H. Fabrication of bismuth subcarbonate nanotube arrays from bismuth citrate. *Chem. Commun.* **2006**, *21*, 2265–2267. [[CrossRef](#)]
10. Cheng, G.; Yang, H.; Rong, K.; Lu, Z.; Yu, X.; Chen, R. Shape-controlled solvothermal synthesis of bismuth subcarbonate nanomaterials. *J. Solid State Chem.* **2010**, *183*, 1878–1883. [[CrossRef](#)]
11. Selvamani, T.; Asiri, A.M.; Al-Youbi, A.O.; Anandan, S. Emergent Synthesis of Bismuth Subcarbonate Nanomaterials with Various Morphologies towards Photocatalytic Activities—An Overview. *Mater. Sci. Forum* **2013**, *764*, 169–193. [[CrossRef](#)]
12. Dong, F.; Lee, S.C.; Wu, Z.; Huang, Y.; Fu, M.; Ho, W.K.; Zou, S.; Wang, B. Rose-like monodisperse bismuth subcarbonate hierarchical hollow microspheres: One-pot template-free fabrication and excellent visible light photocatalytic activity and photochemical stability for NO removal in indoor air. *J. Hazard. Mater.* **2011**, *195*, 346–354. [[CrossRef](#)] [[PubMed](#)]
13. Chen, L.; Huang, R.; Yin, S.F.; Luo, S.L.; Au, C.T. Flower-like $\text{Bi}_2\text{O}_2\text{CO}_3$: Facile synthesis and their photocatalytic application in treatment of dye-containing wastewater. *Chem. Eng. J.* **2012**, *193*, 123–130. [[CrossRef](#)]
14. Cao, X.F.; Zhang, L.; Chen, X.T.; Xue, Z.L. Persimmon-like $(\text{BiO})_2\text{CO}_3$ microstructures: Hydrothermal preparation, photocatalytic properties and their conversion into Bi_2S_3 . *CrystEngComm* **2011**, *13*, 1939–1945. [[CrossRef](#)]
15. Cheng, G.; Wu, J.; Xiao, F.; Yu, H.; Lu, Z.; Yu, X.; Chen, R. Synthesis of bismuth micro- and nanospheres by a simple refluxing method. *Mater. Lett.* **2009**, *63*, 2239–2242. [[CrossRef](#)]
16. Nan, Z.; Chen, X.; Yang, Q.; Wang, X.; Shi, Z.; Hou, W. Structure transition from aragonite to vaterite and calcite by the assistance of SDBS. *J. Colloid Interface Sci.* **2008**, *325*, 331–336. [[CrossRef](#)] [[PubMed](#)]

17. Ni, Z.; Sun, Y.; Zhang, Y.; Dong, F. Fabrication, modification and application of $(\text{BiO})_2\text{CO}_3$ -based photocatalysts: A review. *Appl. Surf. Sci.* **2016**, *365*, 314–335. [[CrossRef](#)]
18. Madhusudan, P.; Zhang, J.; Cheng, B.; Liu, G. Photocatalytic degradation of organic dyes with hierarchical $\text{Bi}_2\text{O}_2\text{CO}_3$ microstructures under visible-light. *CrystEngComm* **2013**, *15*, 231–240. [[CrossRef](#)]
19. Dong, F.; Sun, Y.; Fu, M.; Ho, W.K.; Lee, S.C.; Wu, Z. Novel in situ N-doped $(\text{BiO})_2\text{CO}_3$ hierarchical microspheres self-assembled by nanosheets as efficient and durable visible light driven photocatalyst. *Langmuir* **2012**, *28*, 766–773. [[CrossRef](#)]
20. Dong, F.; Sun, Y.; Ho, W.K.; Wu, Z. Controlled synthesis, growth mechanism and highly efficient solar photocatalysis of nitrogen-doped bismuth subcarbonate hierarchical nanosheets architectures. *Dalton Trans.* **2012**, *41*, 8270–8284. [[CrossRef](#)]
21. Xiong, T.; Huang, H.; Sun, Y.; Dong, F. In situ synthesis of a C-doped $(\text{BiO})_2\text{CO}_3$ hierarchical self-assembly effectively promoting visible light photocatalysis. *J. Mater. Chem. A* **2015**, *3*, 6118–6127. [[CrossRef](#)]
22. Li, S.; Zhang, J.; Chen, X.; Feng, Z.; Li, C. Effect of surface loading and bulk doping of La^{3+} on the thermal stability and photocatalytic activity of $\text{Bi}_2\text{O}_2\text{CO}_3$. *Mater. Res. Bull.* **2017**, *94*, 127–133. [[CrossRef](#)]
23. Li, J.; Liu, Y.; Zhou, Y.; Liu, S.; Liang, Y.; Luo, T.; Dai, G. Enhanced visible-light photocatalytic activity of $\text{Bi}_2\text{O}_2\text{CO}_3$ nanoplates by Fe-doping in the degradation of rhodamine B. *Mater. Res. Bull.* **2018**, *107*, 438–445. [[CrossRef](#)]
24. Zhang, G.Y.; Wang, J.J.; Shen, X.Q.; Wang, J.J.; Wang, B.Y.; Gao, D.Z. Br-doped $\text{Bi}_2\text{O}_2\text{CO}_3$ nanosheets with improved electronic structure and accelerated charge migration for outstanding photocatalytic behavior. *Appl. Surf. Sci.* **2019**, *470*, 63–73. [[CrossRef](#)]
25. Егорышева, А.В.; Краев, А.С.; Гайтко, О.М.; Герасимова, Т.В.; Голодухина, С.В.; Агафонов, А.В. Электрореологические свойства $\alpha\text{-Bi}_2\text{O}_3$ и $\text{Bi}_2\text{O}_2\text{CO}_3$. *Неорганические Материалы* **2019**, *55*, 374–384.
26. Liang, L.; Cao, J.; Lin, H.; Guo, X.; Zhang, M.; Chen, S. Enhancing visible light photocatalytic and photocharge separation of $(\text{BiO})_2\text{CO}_3$ plate via dramatic I⁻ ions doping effect. *Mater. Res. Bull.* **2016**, *80*, 329–336. [[CrossRef](#)]
27. Shen, Z.; Han, Q.; Wang, X.; Zhu, J. Green synthesis of I⁻ ions doped $(\text{BiO})_2\text{CO}_3$ with enhanced visible-light photocatalytic activity. *Mater. Lett.* **2018**, *214*, 103–106. [[CrossRef](#)]
28. Álvarez, L.; Rosas, F.; Márquez, E.; Velasco, E.J. Caracterización y estabilización de la fase metaestable del carbonato de calcio obtenida mediante la aplicación de una capa de $\text{Bi}_2\text{O}_2\text{CO}_3\cdot\text{Al}$ a temperatura ambiente. *Avances Quím.* **2017**, *12*, 13–21.
29. Tobon-Zapata, G.E.; Etcheverry, S.B.; Baran, E.J. Vibrational spectrum of bismuth subcarbonate. *J. Mater. Sci. Lett.* **1997**, *16*, 656–657. [[CrossRef](#)]
30. Cen, W.; Xiong, T.; Tang, C.; Yuan, S.; Dong, F. Effects of morphology and crystallinity on the photocatalytic activity of $(\text{BiO})_2\text{CO}_3$ nano/microstructures. *Ind. Eng. Chem. Res.* **2014**, *53*, 15002–15011. [[CrossRef](#)]
31. Madhusudan, P.; Yu, J.; Wang, W.; Cheng, B.; Liu, G. Facile synthesis of novel hierarchical graphene- $\text{Bi}_2\text{O}_2\text{CO}_3$ composites with enhanced photocatalytic performance under visible light. *Dalton Trans.* **2012**, *41*, 14345–14353. [[CrossRef](#)] [[PubMed](#)]
32. Mohamed, M.; Al, M.; Moamen, S. A novel method for preparation of bismuth(III) carbonate basic $(\text{BiO})_2\text{CO}_3\cdot 3\text{H}_2\text{O}$ upon the reaction of urea with various bismuth(III) salts at high temperature. *Adv. Appl. Sci. Res.* **2012**, *3*, 183–187.
33. Shamaila, S.; Sajjad, A.K.L.; Chen, F.; Zhang, J. Study on highly visible light active Bi_2O_3 loaded ordered mesoporous titania. *Appl. Catal. B Environ.* **2010**, *94*, 272–280. [[CrossRef](#)]

